



## Short communication

One-pot synthesis of three-dimensional  $\text{SnS}_2$  architectures as anode material for lithium-ion batteries

Qiong Wu, Lifang Jiao\*, Juan Du, Jiaqin Yang, Lijing Guo, Yongchang Liu, Yijing Wang, Huatang Yuan

Institute of New Energy Material Chemistry, Key Laboratory of Advanced Energy Materials Chemistry (MOE), Tianjin Key Lab of Metal and Molecule-based Material Chemistry, Nankai University, Tianjin 300071, PR China

## H I G H L I G H T S

- 3D  $\text{SnS}_2$  architectures have been prepared by a facile solvothermal method.
- The evolution process of the architectures has been carefully explored.
- 3D  $\text{SnS}_2$  architectures show superior electrochemical properties.

## A R T I C L E I N F O

## Article history:

Received 24 December 2012

Received in revised form

3 March 2013

Accepted 14 March 2013

Available online 5 April 2013

## Keywords:

Solvothermal synthesis

Tin disulfide

Hierarchitectures

Anode material

Lithium-ion batteries

## A B S T R A C T

Three-dimensional  $\text{SnS}_2$  architectures have been fabricated via a facile solvothermal method. A possible growth mechanism has been propounded based on the time-dependent experiments. As anode material for lithium-ion batteries, the  $\text{SnS}_2$  architectures display long-term cycle stability and excellent high-rate performance. A high specific capacity of  $549.5 \text{ mA h g}^{-1}$  is achieved at a current density of  $100 \text{ mA g}^{-1}$  after 100 discharge/charge cycles. The superior electrochemical performances of  $\text{SnS}_2$  as lithium-ion batteries anode material can be attributed to the synergistic effect of the specific porous structure and the thin nanosheets.

© 2013 Elsevier B.V. All rights reserved.

## 1. Introduction

To solve the energy crisis and environmental contamination, one feasible way is to explore energy storage systems and the forefronts of these systems are electrical energy storage technologies. Undoubtedly, lithium-ion battery has long been considered as one of the most-promising candidates for electric vehicles and portable electronic devices [1]. Graphite, which is commonly used as commercial anode material, could not completely satisfy the needs of the lithium-ion batteries due to the low storage capacity and poor rate performance [2]. To solve this problem, great efforts have been made to develop anode materials as alternatives with elevated storage capacity and longer cycle life for the next generation lithium-ion batteries [3–10].

In recent years,  $\text{SnS}_2$  has sparked considerable attention owing to the unique properties and potential applications. It has been extensively studied in diverse fields, including lithium-ion battery anode material [11–14], adaptive photodetector [15], photoconductor [16], photoluminescence material [17], photocatalyst [18,19], etc. With a layered hexagonal  $\text{CdI}_2$ -type crystal structure ( $a = 0.3648 \text{ nm}$ ,  $c = 0.5899 \text{ nm}$ ),  $\text{SnS}_2$  consists of two layers of close-packed sulfur anions with tin cations sandwiched between them in an octahedral coordination [20]. This layered structure enables the convenient intercalation and exfoliation of  $\text{Li}^+$  [21,22], indicating the potential status of  $\text{SnS}_2$  as anode material for lithium-ion batteries.

Compared with bulk companions, three-dimensional (3D) hierarchical structures with intriguing and superior properties have attracted a great deal of interest [7,23]. To our best knowledge, various  $\text{SnS}_2$  nanostructures, such as nanowalls [24], nanoplates [16,25], nanobelts [26], nanowires [27], aloe-like [28] and leaf-like [29] structures, have been successfully fabricated by template

\* Corresponding author. Tel.: +86 22 23498089; fax: +86 22 23502604.  
E-mail address: [jiaolf@nankai.edu.cn](mailto:jiaolf@nankai.edu.cn) (L. Jiao).

methods, thermal decomposition, chemical bath deposition or microwave-assistant methods and so on. The materials with nanometer-size are favorable in terms of kinetics and capacity, while their practical applications suffer from low thermodynamic stability and high activity toward surface reactions, so hierarchical structures become the best choice which can take both the advantages of nanometer-sized building blocks and micro-sized assemblies [30]. Consequently, the development of feasible and facile approach to manufacture morphology-controlled hierarchical  $\text{SnS}_2$  structures that consist of low-dimensional building blocks is significantly desired.

In this work, we present a one-pot solvothermal process for the preparation of three-dimensional flower-like  $\text{SnS}_2$  hierarchitectures. Compared with previous synthetic methods, we adopt a simple direct means to synthesize well controlled morphologies of  $\text{SnS}_2$  in the absence of templates, catalysts or surfactants. The possible growth mechanism has been proposed by indagating the phase and morphologies of the intermediate products obtained at different reaction times. Moreover, the excellent electrochemical performances of  $\text{SnS}_2$  hierarchitectures manifest that it will be a potential anode material for lithium-ion batteries.

## 2. Experimental

### 2.1. Preparation and structural characterization

All the reagents were used without further purification. 3D flower-like  $\text{SnS}_2$  hierarchitectures are synthesized by a simple solvothermal method. In a typical experiment,  $\text{SnCl}_4 \cdot 5\text{H}_2\text{O}$  (1 mmol) was first dissolved in 68 mL ethanol, and then 2 mL  $\text{CS}_2$  was put into the above solution drop by drop. This solution was transferred into a 100 mL Teflon-lined autoclave with a stainless steel shell. Thereafter, the autoclave was maintained at 160 °C for 24 h and allowed to cool down to room temperature spontaneously. After that, the resulting yellow precipitate was washed with distilled water and ethanol several times and finally dried in a vacuum oven at 80 °C overnight. For comparison study, the reactions with different experimental parameters were repeated while other conditions were kept unchanged.

The crystal phases were identified by X-ray diffraction (XRD, Rigaku.D/Max  $\theta$ ) with a graphite monochromatic  $\text{Cu K}\alpha$  radiation ( $\lambda = 0.15418$  nm) in the  $2\theta$  range from 10° to 80° at room temperature. The morphology and microstructure were observed by scanning electron microscopy (SEM, HITACHI S-4800) and transmission electron microscopy (Tecnai G2 F20 TEM). The Brunauer–Emmett–Teller (BET) specific surface area and pore size distribution of the resultant product were measured with a NOVA 2200e analyzer.

### 2.2. Electrochemical measurements

Electrochemical measurements were performed with the as-synthesized  $\text{SnS}_2$  as the working electrode and lithium metal as the counter/reference electrode. The working electrode was fabricated by mixing 80 wt% of the active material (three-dimensional  $\text{SnS}_2$  hierarchitectures) with 15 wt% conductivity agent (acetylene black) and 5 wt% polymer binder (PVDF) in N-methyl-pyrrolidinone (NMP) solvent to form homogeneous slurry, and then the mixtures were coated on a copper foil. The circular strips were dried at 80 °C for 12 h in vacuum oven. The electrolyte solution obtained by dissolving 1 M  $\text{LiPF}_6$  in the mixture of EC + DMC + EMC (1:1:1 volume ratio) and separator was Celgard 2300 membrane. The testing cells were assembled in an argon-filled glove box with moisture and oxygen contents maintained below 5 ppm. The discharge/charge tests were run on a Land CT2001 automatic battery tester at the

potential range of 0.01–2 V vs.  $\text{Li/Li}^+$ . Cyclic voltammograms (CV) test was performed on a Zahner-Elektrik electrochemical workstation at a scan rate of 0.2  $\text{mV s}^{-1}$  with the voltage ranging from 0 V to 3 V. All the tests were performed at room temperature.

## 3. Results and discussion

### 3.1. Characterization of structure and morphology

The XRD pattern of typical 3D  $\text{SnS}_2$  hierarchitectures is displayed in Fig. 1. We can see that all the strong sharp diffraction peaks can be readily indexed to the standard diffraction data of the corresponding hexagonal  $\text{SnS}_2$  (JCPDS Card File No. 23-677) with a space group of  $P3m1$  and there are no other peaks of the impurities, indicating that the as-obtained  $\text{SnS}_2$  is of high purity and good crystallinity.

The SEM image revealed in Fig. 2a illustrates a flower-like microsphere structure, it is obvious that individual flower-like microsphere is indeed constructed by 2D sheet-like building units, and the mesoporous structure can be also clearly observed. The obtained  $\text{SnS}_2$  exhibits a BET surface area of 47.295  $\text{m}^2 \text{g}^{-1}$  and pore volume of 0.123  $\text{mL g}^{-1}$  by means of nitrogen adsorption–desorption. The pore size distribution indicates the presence of mesopores in the size range of 3–60 nm. The TEM image (Fig. 2b) further confirms the regular flower-like hierarchitectures. Fig. 2c shows the TEM image of the petals of the  $\text{SnS}_2$  flower, the obtained products are assembled by 2D structures with thickness of 50 nm. The relatively light regions in the image correspond to the thin sheets lying along the substrate, while the dark regions signify the nanosheets perpendicularly arranged to the substrate. The HRTEM image (Fig. 2c inset) of the dark region exhibits parallel fringes with an interplanar spacing of about 0.59 nm, which corresponds well to the (001) crystalline plane. In addition, the selected area electron diffraction pattern (SEAD) analysis (Fig. 2d) further confirms single crystalline nature of the  $\text{SnS}_2$ .

### 3.2. Chemical reaction and formation mechanism of the 3D $\text{SnS}_2$ hierarchitectures

As a non-polar organic solvent, it is well known that  $\text{CS}_2$  can dissolve in ethanol to form a homogeneous solution.  $\text{CS}_2$  plays a role of sulfur donor during the whole solvothermal process, in which  $\text{S}^{2-}$  was released as the sulfide source [31].  $\text{Sn}^{4+}$  which dissociates in the ethanol can coordinate with  $\text{S}^{2-}$  to form  $\text{SnS}_2$ . The

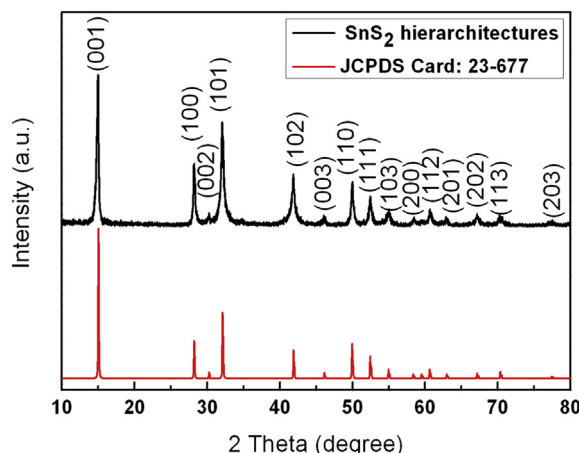


Fig. 1. XRD pattern of  $\text{SnS}_2$  hierarchitectures.

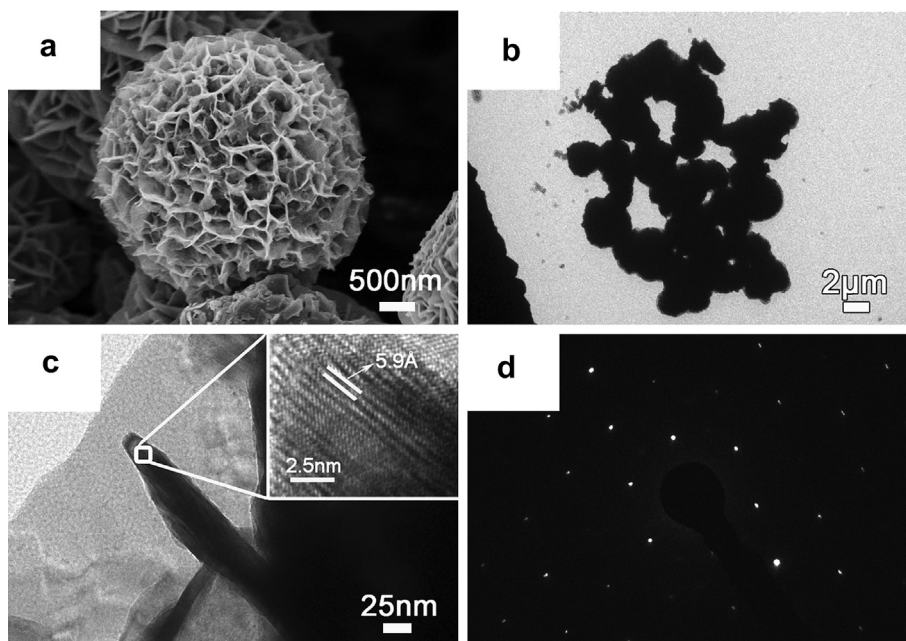
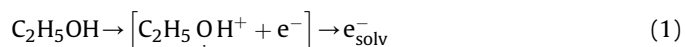


Fig. 2. (a) SEM image, (b, c) TEM images and (d) SAED image of 3D SnS<sub>2</sub> hierarchitectures.

reaction routes for the synthesis of SnS<sub>2</sub> can be expressed as follows:



To further understand the evolution process of the three-dimensional SnS<sub>2</sub> hierarchitectures, a series of experiments have been carried out by adjusting the reaction time. The samples are obtained at different stages of 8 h, 16 h and 32 h. XRD patterns (Fig. 3a) indicate that the intermediate products collected at every time interval can be indexed to hexagonal SnS<sub>2</sub>. With the extension of time, the intensity of the diffraction peaks gradually increases.

Fig. 3b–d also shows the morphology of the samples obtained at different reaction times. The morphology evolution from particles to sheet-like building units can be clearly seen. At the early stage, the sample is composed of irregular nanoparticles (Fig. 3b). The sample collected at 16 h (Fig. 3c) displays an obvious

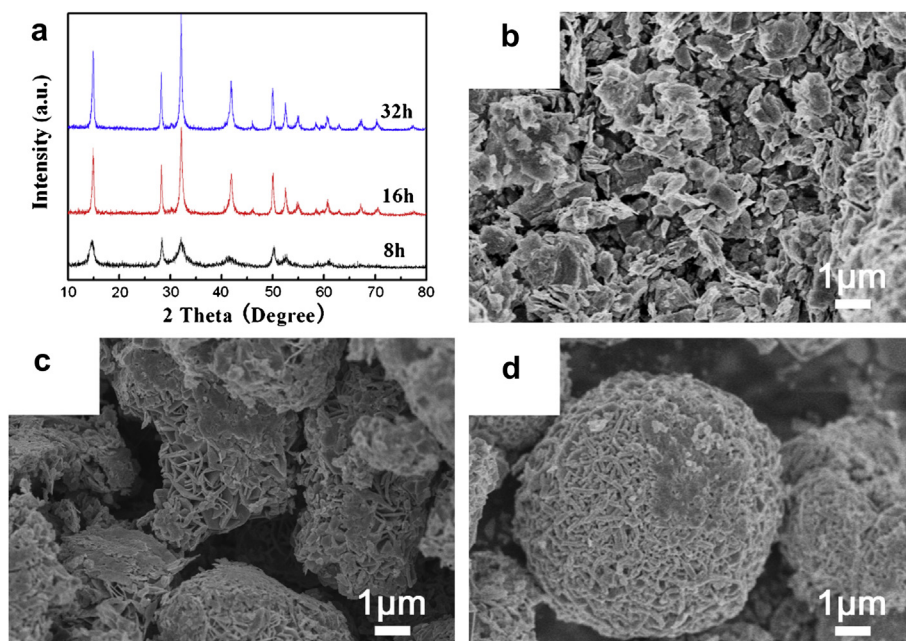


Fig. 3. (a) XRD patterns and (b, c, d) SEM images of the samples synthesized at 160 °C for various dwell times: (b) 8 h, nanoparticles, (c) 16 h, aggregates with irregular nanosheets, (d) 32 h, aggregate spheres with nanorods.

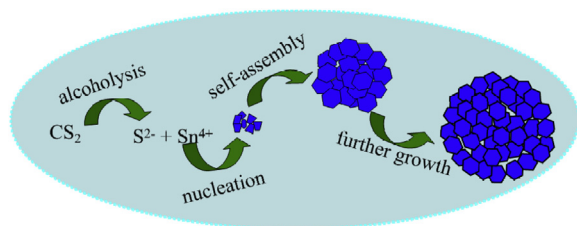


Fig. 4. Schematic illustration of the morphological formation process for the  $\text{SnS}_2$  hierarchitectures.

interconnected petal structure. With the reaction proceeding to 32 h, the mesopores of the microsphere become small owing to the close stacking of the nanosheets (Fig. 3d). Based on the above analysis, we proposed a formation mechanism for the 3D  $\text{SnS}_2$  hierarchitectures. As illustrated in Fig. 4, the growth process involves an initial nucleation stage and a subsequent crystal growth process [32]. In the initial period of the synthesis process, the fast nucleation and congregation of  $\text{SnS}_2$  nanoparticles appear with high concentration of the  $\text{Sn}^{4+}$  and  $\text{S}^{2-}$ . As previously reported [23], these particles may serve as heterogeneous nucleation sites, furnishing the crystalline growth with high-energy sites. With the extension of time, irregular nanoparticles acting as nuclei tend to aggregate spontaneously to form the core of the flower-like structure then grow preferentially with thin sheets, finally forming the 3D flower-like hierarchitectures.

### 3.3. Electrochemical properties

It is widely believed that the morphologies and sizes can affect the electrochemical properties of the electrode materials [33]. The 3D hierarchical structures have many merits in improving electrochemical properties such as larger surface area, greater accessibility to electrolyte, faster transportation of  $\text{Li}^+$ , and accelerated phase transitions [30,34]. We evaluate the as-prepared 3D  $\text{SnS}_2$  hierarchitectures as potential anode material.

The typical CV curves of  $\text{SnS}_2$  hierarchitectures during the first three cycles are demonstrated in Fig. 5a. In the first potential sweeping process, the cathodic peak at 1 V can be attributed to the conversion of  $\text{SnS}_2$  to Sn nanoparticles, along with the formation of  $\text{Li}_2\text{S}$  and the solid electrolyte interphase (SEI) layer. Upon scanning toward more negative direction, the second cathodic peak emerges from 0.25 V to 0 V, owing to the fact that  $\text{Li}^+$  reversibly reacts with Sn metals subsequently. Such peaks can be also observed at the same potential for all cycles. In the anodic process, the deintercalation of  $\text{Li}^+$  from Sn occurs at 0.5–0.7 V. According to the previous report, the additional peak at 2.25 V of anodic peak and 1.75 V of cathodic peak in the first cycle are attributed to the lithium

deintercalation/intercalation of the  $\text{SnS}_2$  layers without causing phase decomposition [35–37]. Obviously, the peak current and peak area decrease along with the cycling, indicating the capacity loss to some degree.

Fig. 5b shows the voltage–capacity profile of the sample for the 1st, 2nd, 3rd, 10th cycle. In the first discharge, the plateau emerging at about 1.25 V is assigned to the decomposition of the  $\text{SnS}_2$ . During the subsequent cycles, the discharge and charge plateaus emerged at potential ranges of 0.0–0.5 V and 0.5–0.7 V vs.  $\text{Li}^+/\text{Li}$  agree with the typical CV profile in Fig. 5a and this result is also corresponding to previously reported in the literature [14,38].

The unfavorable factor affecting the  $\text{SnS}_2$  as anode material is its unsatisfying cyclability. The different morphologies of  $\text{SnS}_2$  have been prepared by researchers to improve the cycle performance. Ma et al. [21] have synthesized  $\text{SnS}_2$  nanoplate with  $540 \text{ mA h g}^{-1}$  after 30 cycles. Hollow spheres were fabricated with the initial reversible capacity of  $592 \text{ mA h g}^{-1}$  and retained  $532 \text{ mA h g}^{-1}$  after 60 cycles at a constant current of  $64.5 \text{ mA g}^{-1}$  [22]. To further improve the cyclability, Kim et al. [39] have synthesized  $\text{SnS}_2$  with uniform carbon layer on surface; still, the discharge capacity only maintained  $668 \text{ mA h g}^{-1}$  after 50 cycles. In view of the merits of 3D hierarchical structures, we tested the lithium storage properties of the  $\text{SnS}_2$  hierarchitectures as anode material for the lithium-ion batteries. On cycling, the irreversible discharge capacity of the first cycle has a high value of  $1837 \text{ mA h g}^{-1}$ . This large irreversible discharge capacity of the first cycle may be caused by the side-reactions of the electrode with electrolytes which result in a large amount of irreversible trapped lithium [40]. The synthesized  $\text{SnS}_2$  electrode still has a large initial reversible capacity of  $1581 \text{ mA h g}^{-1}$  which is much higher than the theoretical reversible capacity ( $645 \text{ mA h g}^{-1}$ ). A continuous capacity fading phenomenon of the electrode is found during the initial 20 cycles. Afterward, the reversibility of cycle performance is getting better, indicating the excellent retention property of the electrode. The discharge capacity is determined to be  $549.5 \text{ mA h g}^{-1}$  after 100 cycles which is much better than previously reported [41–45].

We further investigate the rate property for a better understanding of the advantage of the 3D flower-like  $\text{SnS}_2$  hierarchitectures in lithium-ion battery anode applications. The charge/discharge rates are programmably modified from  $100 \text{ mA g}^{-1}$  to  $200 \text{ mA g}^{-1}$ ,  $500 \text{ mA g}^{-1}$  and  $1000 \text{ mA g}^{-1}$  and then back to  $100 \text{ mA g}^{-1}$  for 10 cycles, as shown in Fig. 6b. Notably, along with the charge/discharge rates, the discharge capacities are measured at  $706.7 \text{ mA h g}^{-1}$ ,  $582.4 \text{ mA h g}^{-1}$ ,  $432.8 \text{ mA h g}^{-1}$ ,  $210.8 \text{ mA h g}^{-1}$ , and reversibly back to  $471 \text{ mA h g}^{-1}$ . The total capacity retention is 73% of the theory reversible capacity. All these experiment results demonstrate the excellent electrochemical properties of 3D flower-like  $\text{SnS}_2$ .

The great storage capacity and excellent stability of the  $\text{SnS}_2$  electrode could ascribe to the specific morphological modification

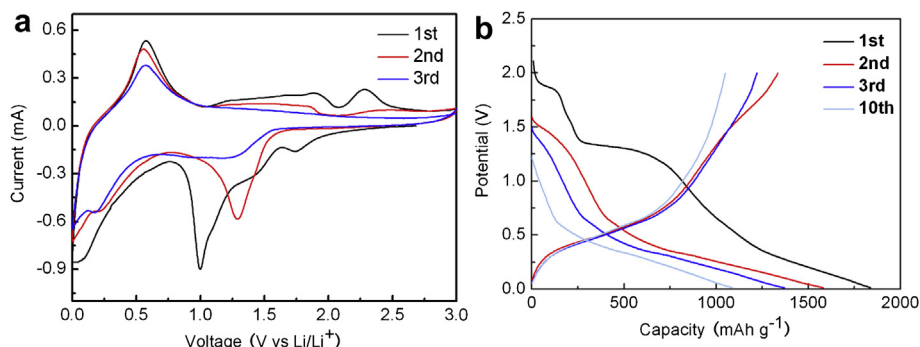


Fig. 5. (a) Cyclic voltammograms (CV) of  $\text{SnS}_2$  hierarchitectures for the first three cycles. (b) The voltage–capacity profiles of  $\text{SnS}_2$  hierarchitectures.

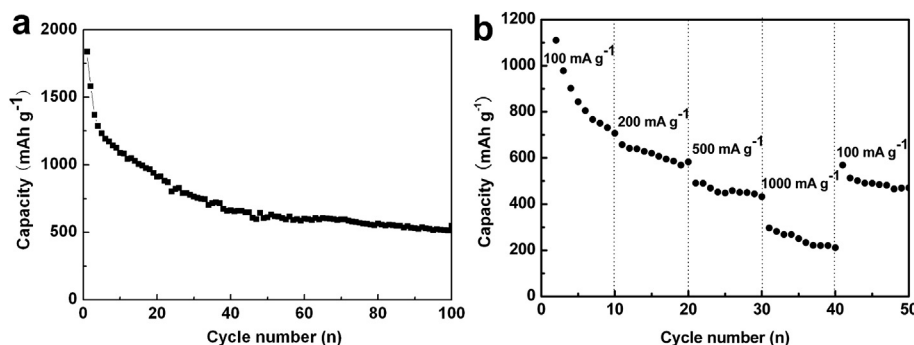


Fig. 6. (a) Cyclic performance of the  $\text{SnS}_2$  hierarchitectures circulated at  $100 \text{ mA g}^{-1}$ . (b) Cyclic performance of  $\text{SnS}_2$  hierarchitectures at different current densities.

of the  $\text{SnS}_2$  combining porous structure with thin nanosheets. First, the specific porous structures are accessible for electrolyte and sufficiently dissipate the mechanical stress stemming from the severe volume change during  $\text{Li}^+$  uptake/removal. Second, owing to the thin nanosheets of  $\text{SnS}_2$ , the diffusion distance is greatly shortened for ionic and electronic transport. These two factors show a distinctive synergetic effect to improve the kinetics of the electrochemical reaction of the  $\text{SnS}_2$  electrode.

#### 4. Conclusions

In this study, 3D  $\text{SnS}_2$  hierarchitectures have been produced via a facile one-pot solvothermal route free of templates and surfactants. The evolution process of the hierarchitectures has also been explored. The as-obtained 3D  $\text{SnS}_2$  hierarchitectures display high discharge capacity and good cycle stability. The high performance of  $\text{SnS}_2$  can be ascribed to its highly hierarchical structures comprised of thin nanosheets. The 3D  $\text{SnS}_2$  hierarchitectures are proved to be a promising material to replace graphite to serve as anode material for the next generation lithium-ion batteries.

#### Acknowledgments

This work was financially supported by 973 program (2010CB631303), NSFC (21073100, 51231003), TSTC (10JCYBJC08000, 11JCYBJC07200, 10SYSYJC27600) and 111 Project (B12015).

#### References

- [1] L.W. Ji, Z. Lin, M. Alcoutlabi, X.U. Zhang, *Energy Environ. Sci.* 4 (2011) 2682–2699.
- [2] V. Etacheri, R. Marom, R. Elazari, G. Salitra, D. Aurbach, *Energy Environ. Sci.* 4 (2011) 3243–3262.
- [3] X.W. Lou, Y. Wang, C.L. Yuan, J.Y. Lee, L.A. Archer, *Adv. Mater.* 18 (2006) 2325–2329.
- [4] S. Boyanov, J. Bernardi, F. Gillot, L. Dupont, M. Womes, J.M. Tarascon, L. Monconduit, M.L. Doublet, *Chem. Mater.* 18 (2006) 3531–3538.
- [5] Y. Lu, Y. Wang, Y.Q. Zou, Z. Jiao, B. Zhao, Y.Q. He, M.H. Wu, *Electrochem. Commun.* 12 (2010) 101–105.
- [6] Y. Wang, J.Y. Lee, *Angew. Chem., Int. Ed.* 45 (2006) 7039–7042.
- [7] J.Q. Yang, L.F. Jiao, Q.Q. Zhao, Q.H. Wang, H.Y. Gao, Q.N. Huan, W.J. Zheng, Y.J. Wang, H.T. Yuan, *J. Mater. Chem.* 22 (2012) 3699–3701.
- [8] Z.Y. Wang, J.S. Chen, T. Zhu, S. Madhavi, X.W. Lou, *Chem. Commun.* 46 (2010) 6906–6908.
- [9] B. Wang, J.S. Chen, H.B. Wu, Z.Y. Wang, X.W. Lou, *J. Am. Chem. Soc.* 133 (2011) 17146–17148.
- [10] Y. Wang, H.C. Zeng, J.Y. Lee, *Adv. Mater.* 18 (2006) 645–649.
- [11] H. Mukaibo, A. Yoshizawa, T. Momma, T. Osaka, *J. Power Sources* 119–121 (2003) 60–63.
- [12] X.L. Gou, J. Chen, P.W. Shen, *Mater. Chem. Phys.* 93 (2005) 557–566.
- [13] T.J. Kim, C. Kim, D. Son, M. Choi, B. Park, *J. Power Sources* 167 (2007) 529–535.
- [14] J.W. Seo, J.T. Jang, S.W. Park, C.J. Kim, B.W. Park, J.W. Cheon, *Adv. Mater.* 20 (2008) 4269–4273.
- [15] I.A. Sokolov, *Measurement* 27 (2000) 13–19.
- [16] T. Shibata, N. Kambe, Y. Muranushi, T. Miura, T. Kishi, *J. Phys. D: Appl. Phys.* 23 (1990) 719–723.
- [17] N.G. Deshpande, A.A. Sagade, Y.G. Gudage, C.D. Lokhande, R. Sharma, *J. Alloys Compd.* 436 (2007) 421–426.
- [18] Y.Q. Lei, S.Y. Song, W.Q. Fan, Y. Xing, H.J. Zhang, *J. Phys. Chem. C* 113 (2009) 1280–1285.
- [19] W.M. Du, D.H. Deng, Z.T. Han, W. Xiao, C. Bian, X.F. Qian, *CrystEngComm* 13 (2011) 2071–2076.
- [20] A. Chakrabarti, J. Lu, A.M. Mcnamara, L.M. Kuta, S.M. Stanley, Z. Xiao, J.A. Maguire, N.S. Hosmane, *Inorg. Chim. Acta* 374 (2011) 627–631.
- [21] J.M. Ma, D.N. Lei, L. Mei, X.C. Duan, Q.H. Li, T.H. Wang, W.J. Zheng, *CrystEngComm* 14 (2012) 832–836.
- [22] J. Xia, G.C. Li, Y.C. Mao, Y.Y. Li, P.K. Shen, L.P. Chen, *CrystEngComm* 14 (2012) 4279–4283.
- [23] Q.H. Wang, L.F. Jiao, H.M. Du, W.X. Peng, Y. Han, D.W. Song, Y.C. Si, Y.J. Wang, H.T. Yuan, *J. Mater. Chem.* 21 (2011) 327–329.
- [24] S. Liu, X.M. Yin, Q.Y. Hao, M. Zhang, L.M. Li, L.B. Chen, Q.H. Li, Y.G. Wang, T.H. Wang, *Mater. Lett.* 64 (2010) 2350–2353.
- [25] Y.Q. Zhu, Y.Q. Chen, L.Z. Liu, *J. Crystal Growth* 328 (2011) 70–73.
- [26] N. Petkov, J. Xu, M.A. Morris, J.D. Holmes, *J. Phys. Chem. C* 112 (2008) 7345–7355.
- [27] Y.T. Lin, J.B. Shi, Y.C. Chen, C.J. Chen, P.F. Wu, *Nanoscale Res. Lett.* 4 (2009) 694–698.
- [28] H.L. Zhu, X. Ji, D.R. Yang, *J. Mater. Sci.* 41 (2006) 3489–3492.
- [29] D.K. Ma, H.Y. Zhou, J.H. Zhang, Y.T. Qian, *Mater. Chem. Phys.* 111 (2008) 391–395.
- [30] Y.G. Guo, J.S. Hu, L.J. Wan, *Adv. Mater.* 20 (2008) 2878–2887.
- [31] Y. Hu, J.F. Chen, W.M. Chen, X.L. Li, *Adv. Funct. Mater.* 14 (2004) 383–386.
- [32] J. Park, V. Privman, E. Matijević, *J. Phys. Chem. B* 105 (2001) 11630–11635.
- [33] C.H. Lai, M.Y. Lu, L.J. Chen, *J. Mater. Chem.* 22 (2012) 19–30.
- [34] P.G. Bruce, B. Scrosati, J.M. Tarascon, *Angew. Chem., Int. Ed.* 47 (2008) 2930–2946.
- [35] C. Julien, C. Perez-Vicente, *Solid State Ionics* 89 (1996) 337–343.
- [36] J. Morales, C. Perez-Vicente, J.L. Tirado, *Solid State Ionics* 51 (1992) 133–138.
- [37] L.H. Zhuo, Y.Q. Wu, L.Y. Wang, Y.C. Yu, X.B. Zhang, F.Y. Zhao, *RSC Adv.* 2 (2012) 5084–5087.
- [38] J.T. Zai, X.F. Qian, K.X. Wang, C. Yu, L.Q. Tao, Y.L. Xiao, J.S. Chen, *CrystEngComm* 14 (2012) 1364–1375.
- [39] H.S. Kim, Y.H. Chung, S.H. Kang, Y.E. Sung, *Electrochim. Acta* 54 (2009) 3606–3610.
- [40] J.T. Zai, K.X. Wang, Y.Z. Su, X.F. Qian, J.S. Chen, *J. Power Sources* 196 (2011) 3650–3654.
- [41] T. Momma, N. Shiraiishi, A. Yoshizawa, T. Osaka, A. Gedanken, J.J. Zhu, L. Sominski, *J. Power Sources* 97–98 (2001) 198–200.
- [42] J.M. Ma, D.N. Lei, X.C. Duan, Q.H. Li, T.H. Wang, A.M. Cao, Y.H. Mao, W.J. Zheng, *RSC Adv.* 2 (2012) 3615–3617.
- [43] C.X. Zhai, N. Du, H. Zhang, D.R. Yang, *Chem. Commun.* 47 (2011) 1270–1272.
- [44] C.X. Zhai, N. Du, H. Zhang, J.X. Yu, D.R. Yang, *Appl. Mater. Interfaces* 3 (2011) 4067–4074.
- [45] B. Luo, Y. Fang, B. Wang, J.S. Zhou, H.H. Song, L.J. Zhi, *Energy Environ. Sci.* 5 (2012) 5226–5230.